Proceedings of the ASME 2020 15th International Manufacturing Science and Engineering Conference
MSEC2020
June 22-26, 2020, Cincinnati, OH, USA

MSEC2020-8477

DESIGN AND EVALUATION OF HUMAN-MACHINE INTERFACE FOR NEXUS: A CUSTOM MICROASSEMBLY SYSTEM

Danming Wei[1], Mariah B. Hall, Andriy Sherehiy, Sumit Kumar Das, Dan O. Popa
Next Generation System Lab, University of Louisville, Louisville, Kentucky

ABSTRACT

Microassembly systems utilizing precision robotics have long been used for realizing 3-dimensional microstructures such as microrobots. Prior to assembly, such components are fabricated using Micro-Electro-Mechanical-System (MEMS) technology. The microassembly system then directs a microgripper through automated or human-controlled pick-and-place operations. In this paper, we describe a novel custom microassembly system, named NEXUS. The NEXUS integrates multi-degree of freedom (DOF) precision positioners, microscope computer vision, and micro-scale process tools such as a microgripper and vacuum tip. A semi-autonomous human-machine interface (HMI) is programmed by NI LabVIEW® to allow the operator to interact with the microassembly system. The NEXUS human-machine interface includes multiple functions, such as positioning, target detection, visual servoing, and inspection. The microassembly system's HMI was used by operators to assemble various 3-dimensional microrobots such as the Solarpede, a novel light-powered stick-and-slip mobile microcrawler. Experimental results are reported in this paper that evaluate the system's semi-autonomous capabilities in terms of assembly rate and yield and compare them to purely teleoperated assembly performance. Results show that the semi-automated capabilities of the microassembly system's HMI offer a more consistent assembly rate of microrobot components.

Keywords: human-machine interface, semi-automated microassembly

1. INTRODUCTION

In the last three decades, robotic microassembly technology has been extensively investigated in a variety of applications of MEMS devices[1-3]. Previously, researchers assembled micro-mechanical components and manipulated biological cells through manual operations[4]. When larger volumes, smaller parts, higher precision, and/or extreme cleanliness are essential to a process, robotic assembly lines or robotic work cells beyond human capabilities are necessary[5]. There is an increasing demand for more complex and versatile microsystems comprised of various materials like Si or GaAs as well as various metals and plastics that will require equally complex assembly[6]. To facilitate interaction between a human user and the machine, researchers have proposed various human-machine interfaces, especially for semi-automated production [7]. A human user can teleoperate and adjust the overall machine system by using the feedback from real-time vision signals. A multi-functional HMI for operating the microassembly system can improve the yield of the assembled products and efficiency of assembly process. Estevez[8] presented a haptic teleoperated microassembly system, which can provide force feedback to human users to achieve superior performance. Probst[2, 3, 9] investigated a full 6 degrees of freedom (DOFs) microassembly system for manufacturing hybrid robotic MEMS devices.

In this paper, we present NEXUS: a 9-DOF microassembly system with a multi-functional human-machine interface (HMI) integrating inverse kinematic function, target inspection, and visual servoing to realize semi-automated assembly for microrobots. This HMI allows an operator to define and control tasks in the Cartesian workspace and two manipulators are used for assembly. An assembly process of the microrobot named Solarpede[10] was chosen to demonstrate NEXUS system HMI capabilities. Fully automated microassembly with the NEXUS is very challenging, due to illumination conditions, MEMS component fabrication uncertainties, environmental conditions such as humidity and surface conditions. On the other hand, manual assembly through teleoperation with human operators is also very challenging and time consuming due to the large

[1] Danming Wei: danming.wei@louisville.edu

number of variables such as positions in 3D space, situational awareness from microscope cameras and so on. The role of a semi-automated HMI is to automate certain parts of the assembly process, while letting the operator perform other tasks manually. We demonstrate that our proposed HMI can greatly improve the operator's assembly rate for Solarpede microrobotic components.

The paper is organized in the following ways: in Section 2, we describe the NEXUS microassembly system and its underlying components; Section 3 details the Solarpede design and operational principles; in Section 4, we discuss the human-machine interface design for the NEXUS microassembly system, and demonstrate how to assemble Solarpede using HMI to realize the semi-automation function; in Section 5, the experimental results are presented, including flexibility and functionality of the NEXUS microassembly system; finally, in Section 6, we conclude the paper and discuss future work.

2. DESIGN OF NEXUS

The NEXUS microassembly system, shown in Figure 1, was designed as a tool for semi-automated assembly of three-dimensional MEMS-based structures and microrobots. It currently consists of two motional manipulators, M1 and M2, and an imaging system consisting of three lenses to monitor the process during microrobot assembly.

1) Manipulator 1 (M1): it is a carrier manipulator which has a sample chuck as the end-effector to hold the sample die. The X and Y-axis manipulations are achieved by two motorized stages Newport® ILS250CC and Newport® 433 series with LTA-HS respectively. The rotational manipulation is performed by a motorized rotation stage Newport® URS75BPP. Integration of three motorized stages results in M1 having 3 DOFs.
2) Manipulator 2 (M2): it is a precise manipulator with a motorized X-Y-Z stage (Newport® VP-25XA-XYZR) and a motorized rotation stage (Newport® PR50CC), as well as a small manual X-Y translation stage. This combination of stages provides 6 (4 plus 2) DOFs. An end-effector with microjammer or microgripper is mounted to the manual X-Y translation stage by the kinematic base (Newport® BK-1A).
3) The imaging system: a top camera (Edmund® EO-3112C) is attached to QIOPTIQ Optem® zoom tube lens combined with stepper motor controller; a side camera (Edmund® EO-0413M) is attached to Edmund® VZM450 zoom imaging lens; a back camera (Edmund® EO-1312C) is attached to Edmund® VZM 100i zoom imaging lens. These three cameras with zoom lenses are used to monitor the assembly process and provide real-time feedback of assembly status. Also, there are three illuminators providing light sources for the imaging systems.

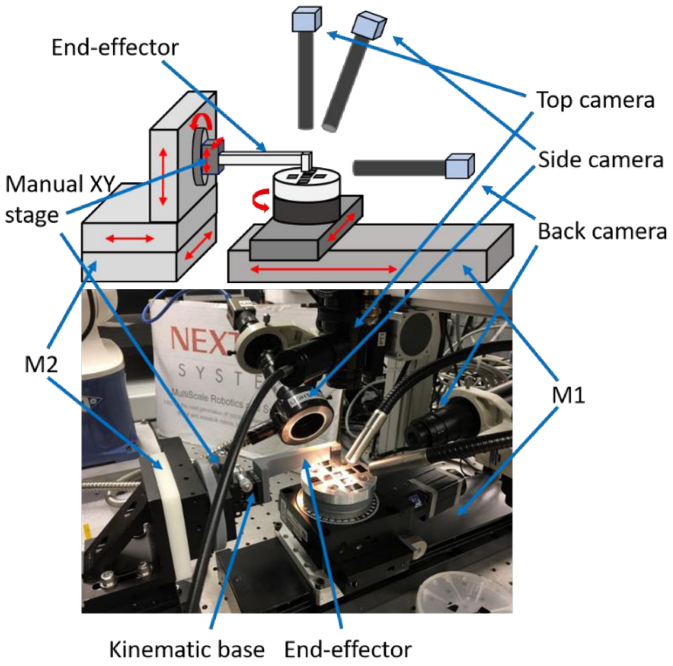

FIGURE 1: NEXUS MICROASSEMBLY SYSTEM SCHEMATIC DIAGRAM AND HARDWARE SETUP

3. DESIGN OF SOLARPEDE MICROROBOT

Solarpede is a novel untethered MEMS microrobot powered by solar cells whose principle of motion is based on the stick-and-slip mechanism. Solarpede is intended to operate as a part of microfactories where it could be a conveyor or transportation system. Solarpede's body consists of the "backpack"– containing solar cells, control circuitry, and motion module – die with MEMS structures. The Solarpede's die consists of eight in-plane chevron electrothermal actuators and eight vertical legs which were fabricated on a silicon-on-insulator (SOI) wafer by using PolyMUMPS and SOI DIRE processes with 100μm thickness device layer[11, 12]. There are two types of leg arrangements on Solarpede's die body as shown in Figure 2: a diagonal leg arrangement (on the left) allows the motion of Solarpede in omni-direction while the parallel leg arrangement (on the right) results in nonholonomic motion of the Solarpede.

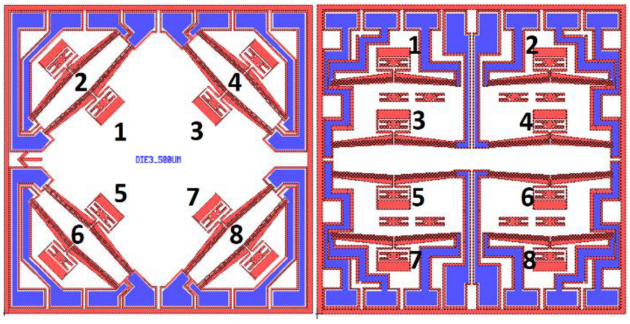

FIGURE 2: SOLARPEDE BODY L-EDIT LAYOUT DESIGN, LEFT: OMNIDIRECTIONAL MOTION; RIGHT: SINGLE DIRECTIONAL MOTION

Solarpede's MEMS legs are assembled perpendicular to the body (die) where they are attached to electrothermal actuator sockets with the help of the Zyvex snap-fastener structures and UV curable adhesive[13, 14]. Figure 3 depicts the dimension of a single leg and socket along with chevron actuator and jammer which is mounted on the end-effector of M1 to pick-and-place the Solarpede's legs.

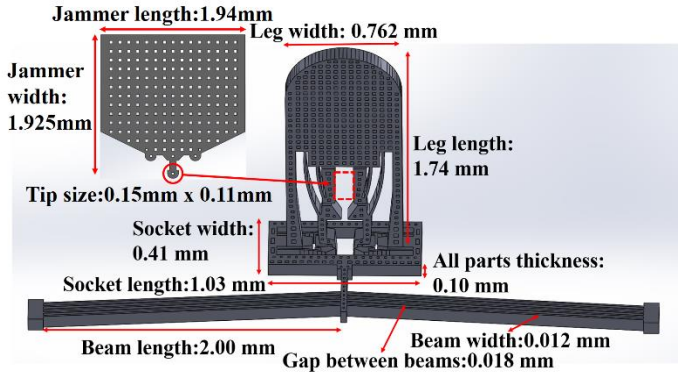

FIGURE 3: DIMENSION OF SINGLE LEG ASSEMBLED INTO THE CHEVRON ACTUATOR AND THE JAMMER

4. HMI DESCRIPTION

The NEXUS human-machine interface, as shown in Figure 5, was developed using NI LabVIEW® and NI Vision Assistant module for the NEXUS microassembly system. NI Vision Assistant is capable of a variety of tasks such as vision acquisition, image processing, and target tracking. As a part of the HMI, those functions allow tracking of specific targets (based on the defined templates) with the help of vision feedback from cameras. The HMI utilizes inverse kinematic functions to assist with coarse adjustment and manipulation of the target. It also includes a target inspection module to filter out viable targets by checking each component of the targets before trying to pick up legs or placing them into the desired sockets. The integrated visual servoing module can assist operators to make fine adjustments to the targets to achieve desired configuration. It also includes a semi-automated function to complete the assembly of microrobots.

The individual modules of the NEXUS HMI are further described in the following subsections.

4.1 Positioning module

In the positioning module, the inverse kinematic function is applied to provide a convenient and reliable operation for the operator. This allows the operator to manipulate the target by sending position and orientation commands and then the interface can calculate the joint commands for the M1 stages. It is necessary for the system's initialization when we try to move a desired target into the field of view (FOV) of the top camera.

To initialize the system, the center of the chuck on M1 is matched to the center of FOV of the top camera. It is recorded as the base frame coordinate (0, 0, 0) representing the linear X-axis, Y-axis, and the rotation θ-axis respectively. Let (x_0, y_0, θ_0) represents an arbitrary point of the desired target on the chuck as shown in Figure 4, then if the target is supposed to rotate a desired orientation θ_2, the target will be moved to a new position (x_1, y_1, θ_1) where $\theta_1 = \theta_0 + \theta_2$. Now if we need to center this point with respect to the top camera, the linear stages have to be displaced linearly by $-x_1$ and $-y_1$ in X and Y directions, respectively. Note that the orientation of the sample chuck will still be maintained at θ_1.

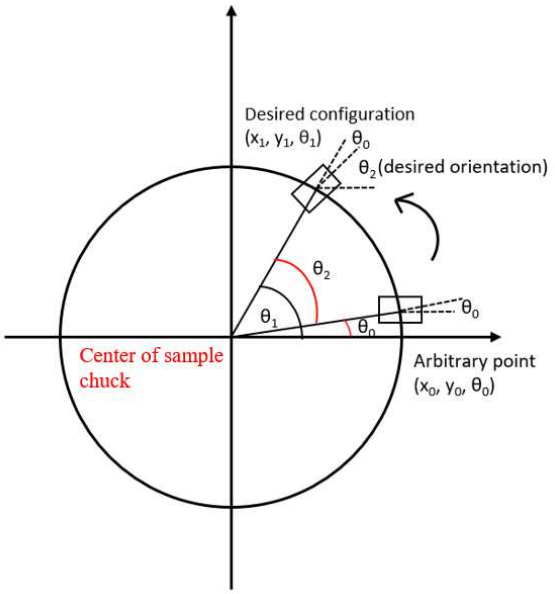

FIGURE 4: ARBITRARY POINT MOVES TO THE DESIRED CONFIGURATION BY INVERSE KINEMATIC FUNCTION [15]

The mathematic relationship between the arbitrary point and its desired configuration is shown in the following equations [15]:

$$\theta_0 = \tan^{-1}(y_0/x_0) \quad (1)$$

$$\theta_1 = \theta_0 + \theta_2 \quad (2)$$

$$x_1 = \sqrt{{x_0}^2 + {y_0}^2}\ \cos\theta_1 \quad (3)$$

$$y_1 = \sqrt{{x_0}^2 + {y_0}^2}\ \sin\theta_1 \quad (4)$$

Based on the above equations, any arbitrary points on the chuck can be moved into the FOV of the top camera. In order to determine the initial coordinates x_0 and y_0 of an arbitrary point of a target, two different coordinate systems are used: chuck coordinate system and individual die layout coordinate system. For example, Figure 6 shows top-left corner coordinates of each die in a chuck's coordinate system where the origin is at the center of sample chuck and, coincidentally, die#1.

After loading the die samples like the distribution of dies in Figure 6, the target point coordinates are determined in die layout coordinate system for specific die (from #1 to #5). Then after translation to the chuck coordinate system, we can define initial coordinates of arbitrary point (x_0 and y_0). Figure 7 depicts four arbitrary points for each different die layout – there are three types of them – with coordinates in die layout coordinate system

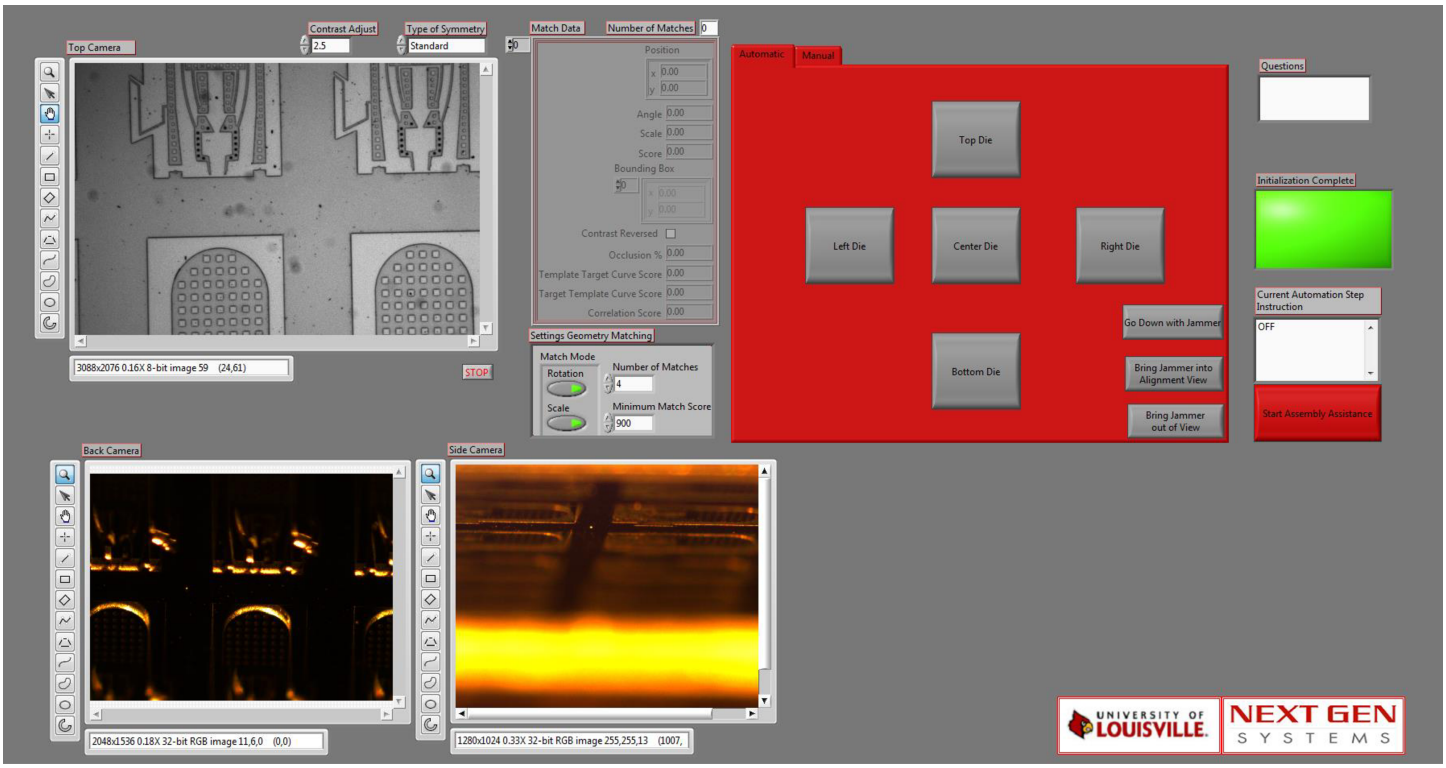

FIGURE 5: THE ENTIRE HUMAN-MACHINE INTERFACE OF NEXUS MICROASSEMBLY SYSTEM

where the origin is in the top-left corner of the die. Table 1 presents coordinates of each arbitrary point in die layout coordinate system for a specific die and corresponding calculated values in chuck coordinate system.

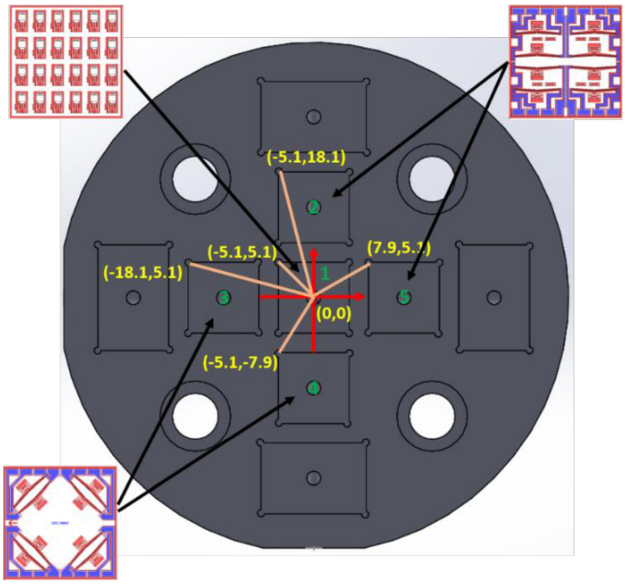

FIGURE 6: DIE DISTRBUTION AND COORDINATES OF TOP-LEFT CORNER REFERRED TO THE ORIGIN ON THE SAMPLE CHUCK

After loading the die samples like the distribution of dies in Figure 6, the target point coordinate should be measured in die layout coordinate system for transferring to the sample chuck coordinate system. Figure 7 indicates that 12 random points of targets selected from three different dies and their coordinates referred to the top-left corner of each die. Table 1 shows each random point coordinate referred to the origin of the sample chuck after calculation.

TABLE 1: RANDOM SELECTED POINTS OF TARGET COORDINATES OF DIE SAMPLES

	No. of points	Coordinates in die layout coordinate system (mm)		Coordinates sample chuck coordinate system (mm)	
		X	Y	X	Y
Die#1 with legs	1	8.938	-1.592	3.838	3.508
	2	7.338	-3.992	2.238	1.108
	3	2.538	-6.392	-2.562	-1.292
	4	0.938	-8.792	-4.162	-3.692
Die#2 with parallel sockets	1	2.321	-1.705	-2.779	16.395
	2	2.321	-3.705	-2.779	14.395
	3	7.387	-5.991	2.287	12.109
	4	7.387	-7.991	2.287	10.109
Die#3 with diagonal sockets	1	8.040	-1.660	-10.060	3.440
	2	6.660	-3.040	-11.440	2.060
	3	1.660	-8.040	-16.440	-2.940
	4	3.040	-6.660	-15.060	-1.560

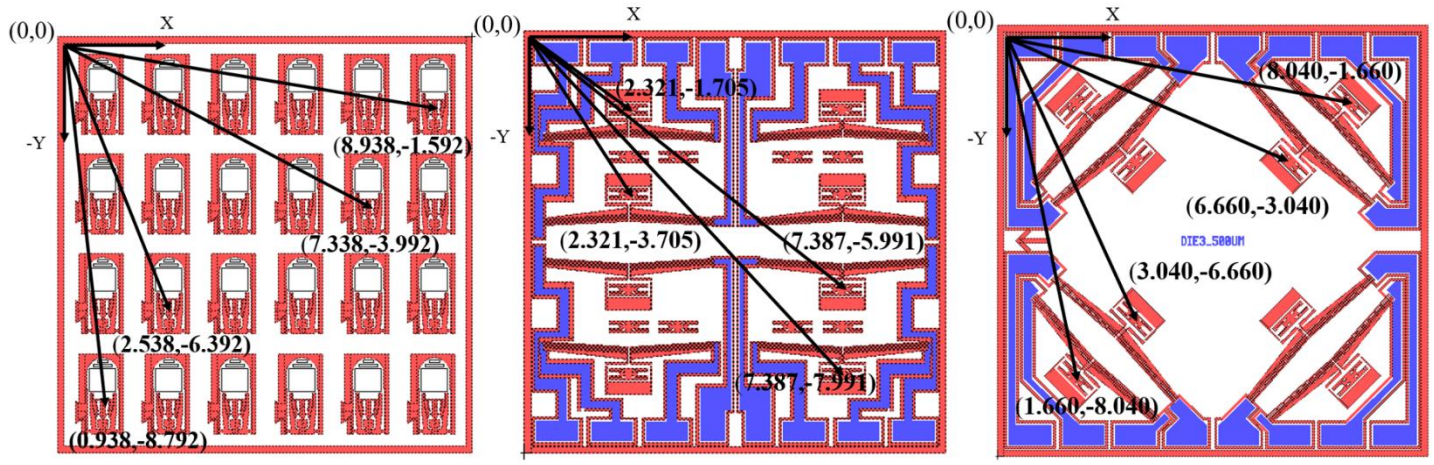

FIGURE 7: THE CENTER OF LEGS AND SOCKETS COORDINATE REFERRED TO THE TOP-LEFT CORNER

In this manner, the initialization procedure can be started when the coordinate of any target's point in chuck coordinate system is entered into NEXUS microassembly system HMI, and then the target can be centered in FOV of the top camera. Naturally, the configuration errors have to be considered during this operation, which we will discuss in Section 5.

4.2 Target detection

Due to the nature of the MEMS fabrication process, MEMS structures will contain dimensional tolerances within a few microns. Target evaluation detection, e.g. estimation of assembly location, have been implemented on the NEXUS human-machine interface. In the case of the Solarpede's leg die, the operator needs to evaluate the structure for viability using visual feedback. Then the leg has to be detected by the interface based on the imported template from the structure's CAD file. If the microstructure is not viable, the operator will move the M1 to the next one. This process repeats until finding the viable leg on a given die. The sequence of the structure testing on a die is from left to right and top to bottom in the top view. For the actuator socket die, the procedure is similar. The sub-interface for target detection has dialogue windows which allows visual inspection of the targets and requires user input regarding structure validity. The operator simply inspects the targets and then clicks the button to select the valid one.

4.3 Visual servoing

After desired target has been selected for the assembly, a fine adjustment becomes an indispensable step in the process. This step is performed using visual servoing, which is based on real-time image signal as feedback to the user to actuate multiple motorized stages to do fine adjustment for a specific feature as a template to move to the desired position.

Visual servoing as a calibration method based on vision feedback for closed-loop control has been employed to enhance the accuracy and flexibilities of the robot system[16-18]. Following the visual servoing theory, in order to accomplish fine adjustment, we employ image Jacobian. With the help of image Jacobian, we can determine the path which the target follows to move to the desired position by step based on target current position. The differences of target center configuration in the top image coordinate in pixel have the relationship with image Jacobian and the configuration of target center differences shown in equation 5. Furthermore, the image Jacobian J' can be expressed in equation 6 as shown below[15]:

$$\begin{bmatrix} \Delta P_x \\ \Delta P_y \\ \Delta P_\theta \end{bmatrix} = J' \begin{bmatrix} \Delta X \\ \Delta Y \\ \Delta \theta \end{bmatrix} \tag{5}$$

$$J' = \begin{bmatrix} J'_{11} & J'_{12} & J'_{13} \\ J'_{21} & J'_{22} & J'_{23} \\ J'_{31} & J'_{32} & J'_{33} \end{bmatrix} \tag{6}$$

where ΔX, ΔY, and Δθ are the variations of the X, Y, and rotation stages in M1; ΔP_x, ΔP_y, and ΔP_θ are variable pixel values of the template in the FOV of the top camera.

After acquiring the image Jacobian, the target motions to the desired position with desired orientation can be planned with the following equation:

$$\begin{bmatrix} X_{new} - X_c \\ Y_{new} - Y_c \\ \theta_{new} - \theta_c \end{bmatrix} = \Delta s \; J'^{-1} \begin{bmatrix} P_{X_d} - P_{X_c} \\ P_{Y_d} - P_{Y_c} \\ P_{\theta_d} - P_{\theta_c} \end{bmatrix} \tag{7}$$

where X_C, Y_C, θ_C, X_{new}, Y_{new}, and θ_{new} are the current and new positions of X, Y, rotation stage of M1, respectively. P_{Xd}, P_{Yd}, $P_{\theta d}$, P_{Xc}, P_{Yc}, and $P_{\theta c}$ are pixel values of the desired and current pose of the assembly template in the FOV of the top camera. Δs is defined as the step size of movement of the M1 stages. Combining inverse kinematic and visual servoing functions of M1, the microstructure can be moved to the desired

configuration with more precision and reliability. Those provide a trusted basement for assembling legs in three-dimensional structure[15].

4.4 Semi-automated assembly

In this section we describe how an operator assembles Solarpede legs using NEXUS-HMI with semi-automated function following Solarpede's leg assembly flow as shown in Figure 8. First, the operator loads dies with the fabricated leg and sockets/actuators on the chuck of M1 (see in Figure 6). Then, the operator can select leg die to move to the FOV of the top camera and then inspect the legs one by one until find the good quality leg; Next, once the leg is selected, it will be moved to the desired position with the desired orientation by using visual servoing function the leg template and ready to be picked up. Then, the jammer mounted on the end-effector of M2 is moved into the FOV of the cameras. The operator controls the jammer to break a tether holding the leg in place on a die. The operator will need to align the jammer tip and pick up the leg by inserting it into the top gripper of the snap-fastener structure. Once the leg is picked up and rotate it in 90-degree., the operator can deposit a pool of UV curable epoxy on the chuck and dip the bottom sides of the leg in it. After the epoxy has been carefully attached to the leg, the jammer with leg is moved out of the FOV of the top camera, then socket die is brought into the view. Each socket is inspected until finding good socket. At this time, the socket template is used to align socket by visual servoing function; Finally, operator control M2 to bring the leg back to the view and place it into the socket to complete the leg assembly. Zyvex snap-fastener's lock mechanism allows the leg to be secured in the socket (with the help of UV epoxy), then the jammer tip will be released. UV light is applied to cure the UV epoxy would ensure the leg's secure attachment to the actuator's socket. The whole leg assembly process combines with manual and automated operations. It can be seen some operations have to be completed by manually, but others can be automatically executed by NI LabVIEW® program, therefore, the NEXUS HMI has capability of semi-automated functions.

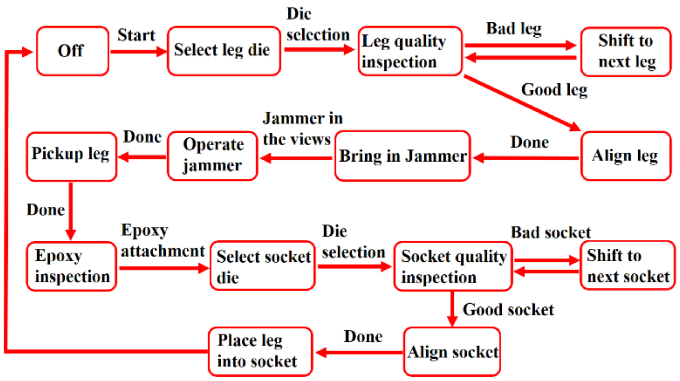

FIGURE 8: BLOCK DIAGRAM OF SOLARPEDE LEG ASSEMBLY FLOW USING THE NEXUS-HMI

5. RESULTS AND DISCUSSION

5.1 Template generation in HMI

In NEXUS HMI, the templates are generated before initiation of the calibration procedure and use of the visual servoing. With NI Vision Assistant, a proper template can be generated after a series of digital imaging processes, like adjusting contrast, brightness, and gamma parameters, and performing color extraction and pattern matching. This step is critical for the target recognition by the Vision Assistant. Figure 9 depicts the generated templates (a for socket and b for leg) which are processed images of specific structures of targets. When the target (socket or leg) is moved to the FOV of the top camera by the positioning module with inverse kinematic function, the template can be recognized by the LabVIEW® program automatically. It has to be noted that during this process configuration errors are always present, so fine calibration has to be done with visual servoing. Template generation is especially important in further development of the full automation of the picking up and placing tasks for the microstructure. It is significantly useful for visual servoing to move the target to the desired position for picking up and placing.

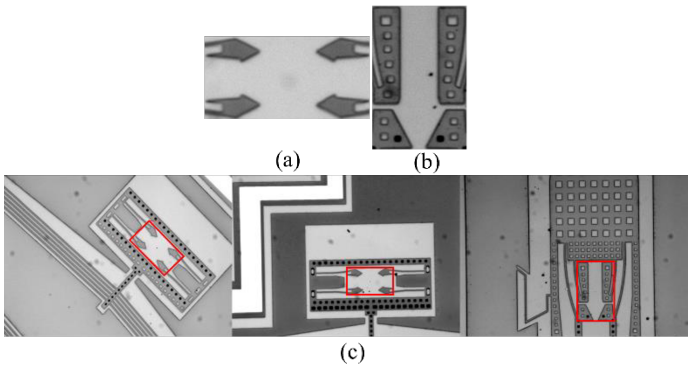

FIGURE 9: (a) AND (b) ARE THE TEMPLATES FOR SOCKET AND LEG RESPECTIVELY; (c) PRESENTS THE TARGETS WITH TEMPLATES MOVING TO THE FOV OF THE TOP CAMERA WITH INVERSE KINEMATIC FUNCTION

5.2 Positioning module calibration

To calibrate inverse kinematic function, we randomly selected 20 points from leg and socket dies following the die distribution in Figure 6. The number of sockets follows the Solarpede body die in Figure 2, the number of legs is counted from left to right and from top to bottom in the leg die, totaling 24 legs. Table 2 presents the configuration errors which occur when the targets (legs and sockets) are supposed to move to the FOV center of the top camera. The measured values received from the images are in pixel, after calculated with fixed magnification of the vertical lens, the ratio between pixel and μm is 1: 0.644. From Table 2, it can be seen that the configuration errors of each die are different because when loading dies on the chuck, each die has different initial configuration with unavoidable errors. However, in the same die, each point has nearly constant configuration errors. Also, those configuration errors are acceptable for NEXUS system, because the goal is to

use the inverse kinematic to move any arbitrary targets on the chuck into the FOV of the top camera and be ready for visual servoing operation.

TABLE 2: CONFIGURATION ERRORS OF RONDOM SELECTED POINTS WHICH ARE SUPPOSED TO THE FOV CENTER OF TOP CAMERA

	No. of sockets or legs	X(μm)	Y (μm)	Θ(deg)
Die#3 diagonal sockets	3	344.97	-65.92	0.69
	4	335.76	-65.35	0.69
	5	367.92	-57.25	0.70
	6	377.80	-52.29	0.70
	Avg.	356.61	-60.20	0.695
Die#4 diagonal sockets	3	414.05	107.60	0.57
	4	417.60	107.21	0.55
	5	431.31	108.62	0.42
	6	424.38	107.62	0.58
	Avg.	421.84	107.76	0.53
Die#2 parallel sockets	1	199.09	204.18	1.03
	3	225.67	203.29	1.03
	6	272.55	143.61	1.07
	8	304.01	147.13	1.03
	Avg.	250.33	174.55	1.04
Die#5 parallel sockets	1	410.08	272.71	0.61
	3	423.97	271.14	0.62
	6	446.76	236.17	0.68
	8	467.52	239.52	0.64
	Avg.	437.08	254.89	0.64
Die#1 legs	6	180.93	284.38	0.82
	11	186.21	287.31	0.78
	14	199.58	301.24	0.73
	19	213.13	307.00	0.78
	Avg	194.96	293.48	0.78

The proper sequence of Solarpede's leg assembly should be considered during operation to avoid possible conflicts and damages. For the Solarpede with parallel arrangement of sockets the assembly sequence is straightforward in order of the assigned socket numbers– from 1 to 10 (see Figure 2). However, for the Solarpede diagonal socket arrangement, there are at least two assembly options: 1) first 4 legs are placed into the 4 inner sockets, and then next 4 legs are placed into the 4 outer sockets; 2) for each corner, the leg is assembled first on the inner socket, followed by the outer socket. Figure 10 displays the successful leg assembled Solarpede dies for both parallel and diagonal socket arrangement.

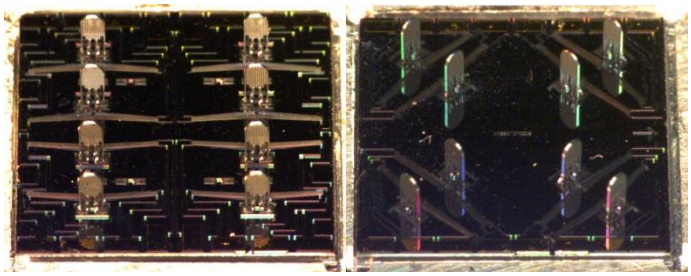

FIGURE 10: ACTUAL SOLARPEDE BODIES WITH EIGHT ASSEMBLED LEGS IN PARALLEL (LEFT) AND DIAGONAL (RIGHT) LEG ARRANGEMENTS

5.3 Evaluation of the Nexus system HMI

To test the efficiency of NEXUS-HMI with semi-automated function, we have designed the experiment where total 50 legs (25-25) have been assembled using NEXUS system in semi-automated (with the help of the HMI assembly assistant) and also in full manual mode (with Newport® XPS controller GUI). Figure 11 presents values of recorded time duration of assembly of single Solarpede's leg in both semi-automated and full manual modes. As it can be seen if we consider all 25 trails on average, the semi-automated assembly was 20% faster and 16% more successful than the manual operation. Although, it has to be noted, it is clearly visible that time duration of assembly in manual mode is decreasing with each trail (from 16 to 18 minutes) where it is comparable with semi-automated mode towards the end of experiment – trails 22-25, in some case it is even lower- trail 12, 18, 19. It can be explained by increased confidence of the NEXUS system operator during the manual mode with the larger number of trails. However due to user's fatigue and human error duration time usually repeatedly increase again. It is also indicated by fluctuations in time duration of assembly for manual mode, that are more significant from trail to trail compared to semi-automated mode we observe more consistent result, where time duration is slightly fluctuating around 8 minutes for all 25 trails.

6. CONCLUSION

In this paper, we introduce a multi-functional semi-automated human machine interface for a custom flexible microassembly system. With inverse kinematic, target detection, and visual servoing functions realized with the help of NI LabVIEW® and NI Vision Assistant module. We have demonstrated that semi-automated human machine interface improves the assembly process of Solarpede microrobot by reducing time, increasing efficiency, and making it more consistent. NEXUS microassembly system can be used for the assembly of the other various types of microrobots or microstructures introducing corresponding modification to the human machine interface. Ultimately presented in this paper, NEXUS HMI can be further developed and upgraded to reach fully automated assembly of the MEMS based microrobots or microstructures, as well as a diverse tool for research on automation and control in the microrobots.

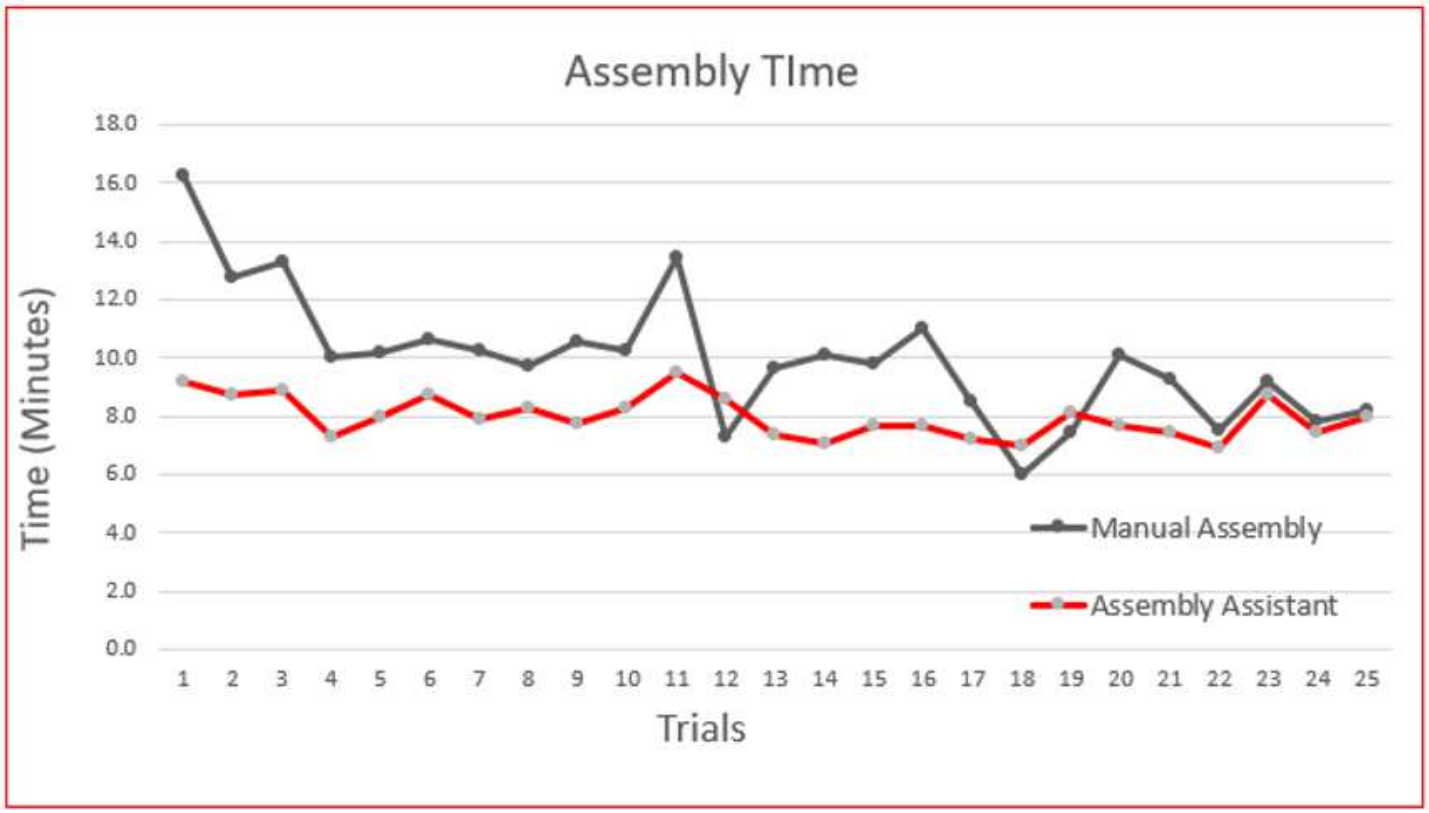

FIGURE 11: COMPARISON OF LEG ASSEMBLY TIME DURATION FOR MANUAL AND SEMI-AUTOMATED OPERATION

ACKNOWLEDGEMENTS

This work was supported by National Science Foundation under grant MRI #1828355 and Kentucky EPSCOR RII-Track-1 project #1849213. We would like to thank the staff of University of Louisville's Micro Nano Technology Center (MNTC) for their great suggestion and help in fabricating Solarpede components.

REFERENCES

[1] Xie, H., Rong, W., Sun, L., and Chen, L., "A flexible microassembly system for automated fabrication of MEMS sensors," Proc. 2006 9th International Conference on Control, Automation, Robotics and Vision, IEEE, pp. 1-6.

[2] Probst, M., Hürzeler, C., Borer, R., and Nelson, B. J., 2009, "A microassembly system for the flexible assembly of hybrid robotic mems devices," International Journal of Optomechatronics, 3(2), pp. 69-90.

[3] Probst, M., Borer, R., and Nelson, B. J., "A microassembly system for manufacturing hybrid mems," Proc. Proceedings of the 12th IFToMM World Congress, IFToMM.

[4] Huang, X., Lv, X., and Wang, M., "Development of a robotic microassembly system with multi-manipulator cooperation," Proc. 2006 International Conference on Mechatronics and Automation, IEEE, pp. 1197-1201.

[5] Hollis, R. L., and Rizzi, A. A., "Agile assembly architecture: A platform technology for microassembly," Proc. Proc. Am. Soc. for Precision Engineering 19th Annual Meeting, Orlando.

[6] Cohn, M. B., Boehringer, K. F., Noworolski, J. M., Singh, A., Keller, C. G., Goldberg, K. A., and Howe, R. T., "Microassembly technologies for MEMS," Proc. Microelectronic Structures and MEMS for Optical Processing IV, International Society for Optics and Photonics, pp. 2-16.

[7] Langer, M., and Söffker, D., "Human guidance and supervision of a manufacturing system for semi-automated production," Proc. 2011 IEEE Jordan Conference on Applied Electrical Engineering and Computing Technologies (AEECT), IEEE, pp. 1-6.

[8] Estevez, P., Khan, S., Lambert, P., Porta, M., Polat, I., Scherer, C., Tichem, M., Staufer, U., Langen, H. H., and Schmidt, R. M., "A Haptic Tele-operated system for Microassembly," Proc. International Precision Assembly Seminar, Springer, pp. 13-20.

[9] Probst, M., Vollmers, K., Kratochvil, B. E., and Nelson, B. J., "Design of an advanced microassembly system for the automated assembly of bio-microrobots," Proc. Proc. 5th International Workshop on Microfactories, Citeseer.

[10] Klotz, J. F., Wei, D., Yang, Z., Zhang, R., Sherehiy, A., Saadatzi, M. N., and Popa, D. O., "Concept Validation for a

Novel Stick-and-Slip, Light-Powered, Mobile Micro-Crawler," Proc. 2019 International Conference on Manipulation, Automation and Robotics at Small Scales (MARSS), IEEE, pp. 1-7.
[11] Pac, M. R., and Popa, D. O., "3-DOF untethered microrobot powered by a single laser beam based on differential thermal dynamics," Proc. 2011 IEEE International Conference on Robotics and Automation, IEEE, pp. 121-127.
[12] Que, L., Park, J.-S., and Gianchandani, Y. B., 2001, "Bent-beam electrothermal actuators-Part I: Single beam and cascaded devices," Journal of Microelectromechanical Systems, 10(2), pp. 247-254.
[13] Park, J.-S., Chu, L. L., Oliver, A. D., and Gianchandani, Y. B., 2001, "Bent-beam electrothermal actuators-Part II: Linear and rotary microengines," Journal of Microelectromechanical systems, 10(2), pp. 255-262.
[14] Tsui, K., Geisberger, A. A., Ellis, M., and Skidmore, G. D., 2004, "Micromachined end-effector and techniques for directed MEMS assembly," Journal of Micromechanics and Microengineering, 14(4), p. 542.
[15] Wei, D., 2018, "Challenges in flexible microsystem manufacturing: fabrication, robotic assembly, control, and packaging."
[16] Hashimoto, K., 1993, Visual servoing: real-time control of robot manipulators based on visual sensory feedback, World scientific.
[17] Hutchinson, S., Hager, G. D., and Corke, P. I., 1996, "A tutorial on visual servo control," IEEE transactions on robotics and automation, 12(5), pp. 651-670.
[18] Fang, Y., Dawson, D., Dixon, W., and Dequeiroz, M., "2.5 D visual servoing of wheeled mobile robots," Proc. Proc. of the IEEE Conference on Decision and Control, Las Vegas, NV, Citeseer.